Applied Physics Letters ARTICLE pubs.aip.org/aip/apl

High conductivity coherently strained quantum well XHEMT heterostructures on AlN substrates with delta doping

Cite as: Appl. Phys. Lett. **125**, 142110 (2024); doi: 10.1063/5.0228253
Submitted: 11 July 2024 · Accepted: 22 September 2024 ·
Published Online: 3 October 2024

View Online

Export Citation

CrossMark

Yu-Hsin Chen,[1,a)] Jimy Encomendero,[2] Chandrashekhar Savant,[1] Vladimir Protasenko,[2] Huili (Grace) Xing,[1,2,3] and Debdeep Jena[1,2,3]

AFFILIATIONS

[1]Department of Materials Science and Engineering, Cornell University, Ithaca, NY 14853, USA
[2]School of Electrical and Computer Engineering, Cornell University, Ithaca, NY 14853, USA
[3]Kavli Institute at Cornell for Nanoscale Science, Cornell University, Ithaca, NY 14853, USA

[a)]Author to whom correspondence should be addressed: yc794@cornell.edu

ABSTRACT

Polarization-induced two-dimensional electron gases (2DEGs) in AlN/GaN/AlN quantum well high-electron-mobility transistors on ultra-wide bandgap AlN substrates offer a promising route to advance microwave and power electronics with nitride semiconductors. The electron mobility in thin GaN quantum wells embedded in AlN is limited by high internal electric field and the presence of undesired polarization-induced two-dimensional hole gases (2DHGs). To enhance the electron mobility in such heterostructures on AlN, previous efforts have resorted to thick, relaxed GaN channels with dislocations. In this work, we introduce n-type compensation δ-doping in a coherently strained single-crystal (Xtal) AlN/GaN/AlN heterostructure to counter the 2DHG formation at the GaN/AlN interface, and simultaneously lower the internal electric field in the well. This approach yields a δ-doped XHEMT structure with a high 2DEG density of $\sim 3.2 \times 10^{13}$ cm^{-2} and a room temperature (RT) mobility of $\sim$ 855 cm^2/Vs, resulting in the lowest RT sheet resistance 226.7 $\Omega/\square$ reported to date in coherently strained AlN/GaN/AlN HEMT heterostructures on the AlN platform.

Published under an exclusive license by AIP Publishing. https://doi.org/10.1063/5.0228253

Ultrawide bandgap AlN-based quantum well (QW) high-electron-mobility transistors (HEMTs) offer a promising alternative platform for high-power and high-frequency amplifiers.[1,2] This structure features a thin, coherently and compressively strained GaN QW enclosed between an unstrained top AlN barrier, and a thick, unstrained epitaxial AlN buffer layer. The high thermal conductivity of the AlN buffer layer[3] improves heat dissipation, while its ultra-wide energy bandgap provides electrical insulation, eliminating the need for compensation doping in the buffer layer. Additionally, this wide bandgap improves the breakdown electric field in the devices.[4,5] The large polarization discontinuity between AlN and GaN induces a two-dimensional electron gas (2DEG), and the large conduction band offset between AlN and GaN confines the 2DEG in the QW.[6] While such AlN/GaN/AlN heterostructures can be realized on SiC, Si, or sapphire substrates, the highest performance transistors are attainable in HEMTs or XHEMTs on single-crystal (Xtal) AlN substrates because of a $\sim$ millionfold decrease in dislocation density,[7,8] and the near elimination of the thermal boundary resistance with the substrate.[9]

Though 2DEGs in AlN/GaN/AlN heterostructures have exhibited respectable 2DEG densities of $n_s \sim 2-3 \times 10^{13}$ cm^{-2}, they exhibit lower room temperature (RT) electron mobilities $\mu \sim 600$ cm^2/Vs and comparable sheet resistances $R_s \sim 400$–$500\,\Omega/\square$[10–14] to conventional AlGaN/GaN HEMTs on relaxed GaN layers ($\mu \sim 1500$ cm^2/Vs, $n_s \sim 10^{13}$ cm^{-2} and $R_s \sim 400\,\Omega/\square$). The electron mobility in AlN/GaN/AlN heterostructures is currently limited by two factors: (1) A strong internal electric field in the well,[15,16] and (2) a polarization-induced two-dimensional hole gas (2DHG)[17,18] that coexists with 2DEG in the same QW, confined by the valence band offset between AlN and GaN at the opposite interface of the 2DEG. This 2DHG can degrade the measured apparent 2DEG mobility by parallel conduction.[14,19–21] In narrow wells, the close proximity of the bilayer can cause Coulomb drag, resulting in further reduction of electron mobility.[22] For n-channel transistor operation, the empty electron states (holes in the 2DHG) in the valence band can trap electrons from the channel and release them slowly, causing the ac current to be lower than in dc, degrading transistor performance.

03 October 2024 12:12:56

In a recent study of AlN/GaN/AlN heterostructures on single-crystal AlN substrates,[23] enhancing RT electron mobility to over 1000 cm^2/Vs was achieved by reducing the vertical electric field by increasing the GaN QW thickness to its relaxed form. The drawback of this approach is the introduction of dislocations in the GaN channel. In this work, we present a distinct XHEMT design which incorporates n-type compensation δ-doping in a coherently strained QW. The δ-doping (1) removes the polarization-induced 2DHG in the QW, and (2) reduces the internal electric field in the well. The approach is similar in spirit to n-type doping in N-polar GaN HEMTs on GaN, where it eliminates undesired 2DHGs and positively charged donor traps. The trap states have been accused of causing dispersion[24] and anomalous output conductance[25] in HEMTs, and of degrading the quantum efficiency of light emitting diodes.[26]

The key criterion to prevent these effects hinges on designing a heterostructure that pulls the valence band edge E_v sufficiently below the Fermi level E_F to eliminate 2DHG formation and to ensure trap states remain filled. We epitaxially grew undoped QW HEMT and δ-doped XHEMT heterostructures on Al-polar single-crystal AlN substrates, as depicted in Figs. 1(a) and 1(b). The thickness of each layer is kept identical for both samples to focus on the impact of δ-doping. We first calculated the energy band diagram and carrier density for both structures by using a self-consistent Schrödinger–Poisson solver with a surface barrier height of 0.5 eV, neglecting defects and traps. The energy band diagram of the undoped QW HEMT structure in Fig. 1(c) shows the high polarization-induced electric field in the 20 nm GaN QW. Figure 1(e) shows that at the top AlN/GaN heterojunction $\sim$7 nm below the surface, a net positive polarization sheet charge induces a mobile 2DEG with a density of $n_s = 2.23 \times 10^{13}$ cm^{-2}, whereas at the bottom GaN/AlN heterojunction $\sim$27 nm below the surface, a net negative polarization sheet charge induces a mobile 2DHG with a density of $p_s = 3.91 \times 10^{13}$ cm^{-2}.

Figure 1(d) shows the calculated energy band diagram of the δ-doped XHEMT structure introduced in this work. We applied δ-doping within the GaN QW, 1 nm away from the GaN/AlN buffer interface, $\sim$26 nm below the surface. Introducing δ-doping with donor density of $\sigma_\delta = 4 \times 10^{13}$ cm^{-2} does not completely remove the 2DHG. Increasing the doping to $\sigma_\delta = 5 \times 10^{13}$ cm^{-2} pulls E_v completely below E_F, and keeps E_F inside the energy gap. Further increasing the doping density to $\sigma_\delta = 6 \times 10^{13}$ cm^{-2} results in the formation of an undesired second electron channel and $E_F > E_c$ at the delta-doping plane. Following these calculations, we grew a series of samples with varying σ_δ. The 2DEG density increases with higher doping density. The electron mobility remains relatively unchanged at low δ-doping density. The sample with $\sigma_\delta = 5 \times 10^{13}$ cm^{-2} indeed exhibited the lowest sheet resistance and highest electron mobility. In contrast, the sample with higher δ-doping density shows a decline in electron mobility, likely due to the parallel conduction in the QW. In

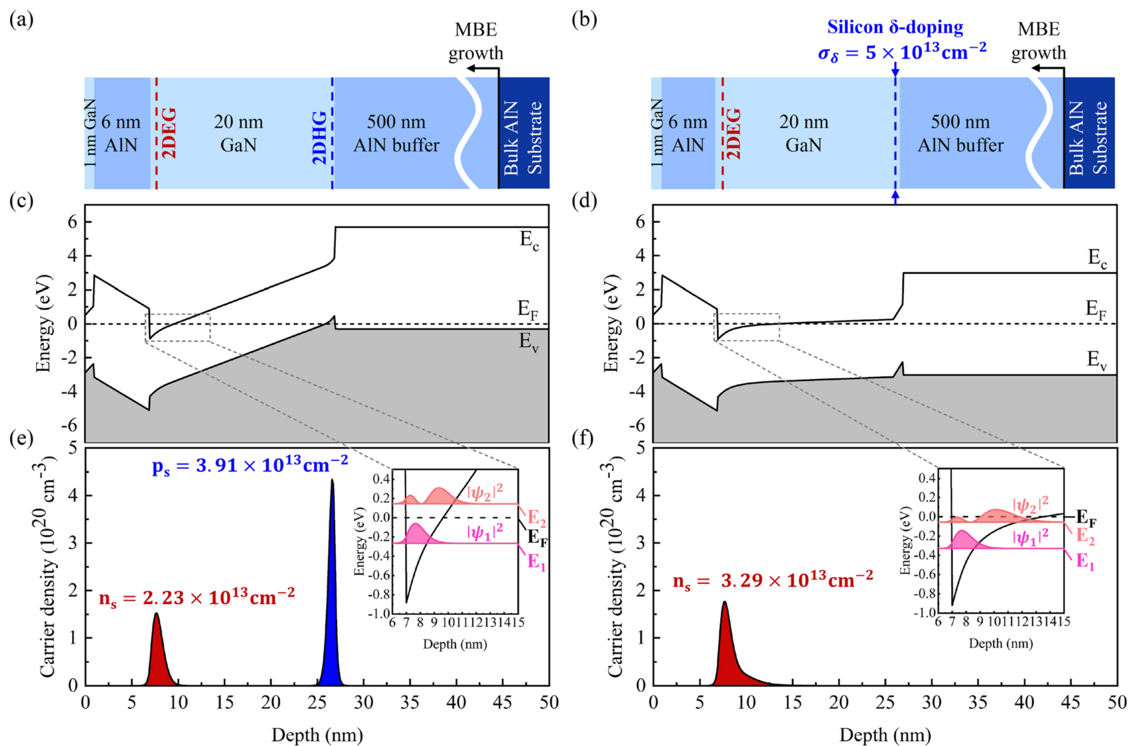

FIG. 1. (a) Schematic of the epitaxial undoped AlN/GaN/AlN QW HEMT heterostructure. (b) δ-doped AlN/GaN/AlN XHEMT heterostructure includes a sheet of n-type donors σ_δ. (c) and (d) Simulated energy-band diagrams of the undoped QW HEMT and δ-doped XHEMT heterostructures, respectively. Incorporating δ-doping with a donor density of $\sigma_\delta = 5 \times 10^{13}$ cm^{-2} shifts the valence band E_v farther below the Fermi level E_F. (e) and (f) Simulated carrier density profile of the undoped QW HEMT and δ-doped XHEMT, respectively. High-density 2DEG is confined at the top AlN/GaN interface $\sim$7 nm below the surface. N-type δ-doping eliminates the presence of 2DHG at the GaN/AlN interface $\sim$27 nm below the surface. The insets in panels (e) and (f) show the energy of the electronic subbands and the squared-amplitude of the electronic wavefunctions in the undoped QW HEMT and δ-doped XHEMT heterostructures, respectively.

03 October 2024 12:12:56

Published under an exclusive license by AIP Publishing

the rest of this work, we discuss the structural and electronic transport properties of the optimal δ-doped XHEMT with $\sigma_\delta = 5 \times 10^{13}$ cm^{-2}, comparing it with the undoped QW HEMT ($\sigma_\delta = 0$), and leave detailed studies of the extended series to a future work.

Figures 1(d) and 1(f) show that $\sigma_\delta = 5 \times 10^{13}$ cm^{-2} eliminates the 2DHG, reduces the internal electric field in the QW, and shifts E_v far below E_F compared to the undoped structure in Fig. 1(c), where $E_F < E_v$ at $\sim$27 nm below the surface. The reduced internal electric field moves the centroid of the 2DEG away from the interface at $\sim$7 nm below the surface. This is expected to decrease interface roughness (IR) scattering and enhance the electron mobility.[27,28] Hall effect measurements reveal that the δ-doped XHEMT exhibits a 2DEG density of $n_s = 3.24 \times 10^{13}$ cm^{-2} and RT electron mobility of $\mu = 854.6$ cm^2/Vs, resulting in a RT sheet resistance of $R_s = 226.7\,\Omega/\square$. In contrast, the undoped QW HEMT experimentally exhibits a higher RT $R_s = 501.9\,\Omega/\square$, with $n_s = 2.04 \times 10^{13}$ cm^{-2} and RT $\mu = 611.1$ cm^2/Vs. The XHEMT achieves a $>$ 2X lower sheet resistance compared to the undoped QW HEMT structure.

We used a Veeco GEN10 molecular beam epitaxy (MBE) system equipped with a nitrogen radio frequency (RF) plasma source and Al, Ga and Si standard effusion cells to grow the AlN/GaN/AlN heterostructures shown in Figs. 1(a) and 1(b). These heterostructures were grown on single-crystal AlN substrates with dislocation densities less than 10^4 cm^{-2} from Crystal IS.[29] Prior to epitaxial growth, the single-crystal AlN substrates underwent essential cleaning steps described in our earlier work.[30] After *ex situ* cleaning in solvents and acids, we loaded the diced AlN substrates into the MBE system, outgassed them at 200 °C for 7 h, and performed *in situ* Al-assisted surface cleaning, which involves repeated cycles of aluminum adsorption and desorption to remove the native surface oxide and allow high-quality homoepitaxy.[30,31]

After the cleaning process, we grew a 500 nm homoepitaxial AlN buffer layer under metal-rich conditions and at a thermocouple temperature of $T_c = 1060$ °C to ensure step-flow growth mode and high crystallinity. We then thermally desorbed excess Al droplets *in situ*. Subsequently, we grew the active region continuously, consisting of a 20 nm GaN QW, 6 nm AlN barrier, and 1 nm GaN cap, under metal-rich conditions and without any growth interruptions. This was done with the RF plasma power of 200 W and a N_2 gas flow of 0.35 sccm, corresponding to a growth rate of 0.2 μm/h. For the undoped QW HEMT, we held the substrate for the active region at a thermocouple temperature $T_c = 850$ °C. For the δ-doped XHEMT, we adjusted it to $T_c = 820$ °C to ensure the presence of Ga droplets on the surface during the δ-doping process. Silicon δ-doping was incorporated after deposition of 1 nm GaN. We calibrated the δ-doping condition using a separate MBE-grown silicon-doped GaN sample using a silicon cell temperature of 1195 °C, yielding a 3D doping density of 1.23×10^{19} cm^{-3}. During δ-doping, we opened the silicon shutter while keeping the Ga and N shutters closed and the N_2 plasma on, for the time needed to achieve $\sigma_\delta = 5 \times 10^{13}$ cm^{-2}. The silicon doping level in a separate δ-doped XHEMT was experimentally confirmed using secondary ion mass spectrometry (SIMS) by the Evans Analytical Group to be $\sigma_\delta = 5.5 \times 10^{13}$ cm^{-2}. Once the δ-doping process was completed, we promptly opened the Ga and N shutters to resume the growth of the remaining 19 nm GaN QW and subsequent layers. After the epitaxial growth, we cooled down the substrates immediately to RT and removed excess Ga droplets *ex situ* using HCl.

We assessed the structural quality of the heterostructures by high-resolution x-ray diffraction (HRXRD) with a Panalytical Empyrean® diffractometer emitting Cu K$_{\alpha1}$ radiation (1.54 Å). The solid lines in Fig. 2(a) show the measured diffraction patterns of both samples around the (002) symmetric reflection. The dashed red lines in Fig. 2(a) are the theoretical diffraction patterns calculated using a dynamical diffraction model. Clearly resolved interference fringes suggest sharp heterointerfaces. We extracted the thicknesses of each layer from the good agreement between the measured and calculated diffraction patterns, showing precise control over thicknesses. Both the undoped and δ-doped samples consist of the following layer structure: 1 nm GaN cap/6 nm AlN barrier/20 nm GaN channel/500 nm AlN buffer grown on top of a single-crystal AlN substrate. The reciprocal space maps (RSMs) around the asymmetric ($-$105) diffraction in Figs. 2(b) and 2(c) show coherently strained GaN layers throughout both heterostructures. This implies that silicon incorporation has no measurable structural impact on the strain of the film. The estimated dislocation density in such heterostructure is expected to be similar to that of the substrate, as no additional dislocations are introduced due to the strained GaN QW layer. We characterized the surface morphologies using atomic force microscopy (AFM) with an Asylum Research Cypher ES setup. Figures 2(d) and 2(e) show atomic steps, suggesting step-flow growth mode. Additionally, the sub-nanometer root mean square (rms) roughnesses indicate smooth surface morphologies.

We conducted temperature-dependent Hall effect measurements using a Van der Pauw geometry with soldered indium dots as Ohmic contacts. The carrier concentration n_s, mobility μ, and sheet resistance R_s—at 290 and 10 K—are summarized in Table I and shown in Fig. 3. Figure 3(a) shows that the 2DEG sheet densities of both the undoped and δ-doped samples remain unchanged down to cryogenic temperatures, confirming their polarization-induced origin. Silicon δ-doping is seen to increase the 2DEG density from 2.04×10^{13} cm^{-2} in the undoped case to 3.24×10^{13} cm^{-2} in the XHEMT due to modulation doping effect. Electrons supplied by donors end up in three locations: (1) They compensate the 2DHG and any traps near the bottom GaN/AlN interface $\sim$27 nm below the surface. (2) Most of the remaining electrons end up in the QW near the top AlN/GaN interface $\sim$7 nm below the surface, where they become confined and contribute to conductivity. Consequently, the internal electric field in the well decreases, resulting in flattened energy bands and lower subband energies. (3) A small portion of the donor electrons can end up on the surface to help the system achieve thermal equilibrium.

In the inset of Fig. 1(e), the calculated energy band diagram and electronic subband energies of the undoped structure result in a single subband occupation, with its ground state energy E_1 positioned 0.266 eV below E_F. In contrast, the δ-doped XHEMT has two subbands occupied as shown in the inset of Fig. 1(f). The second subband minimum E_2, located only 0.056 eV below E_F, is relatively shallow. The majority of electrons at this AlN/GaN heterojunction also occupy the first subband, with its minimum E_1 situated 0.33 eV below E_F. The experimentally measured 2DEG densities for both heterostructures are close to the calculated densities from a self-consistent Schrödinger–Poisson solver with a surface barrier height of 0.5 eV.

Figure 3(b) shows that the mobilities measured in both samples increase monotonically with decreasing temperature due to phonon freeze out. At low temperatures, the mobility saturates due to temperature-independent IR scattering. The RT mobility increases

03 October 2024 12:12:56

Published under an exclusive license by AIP Publishing

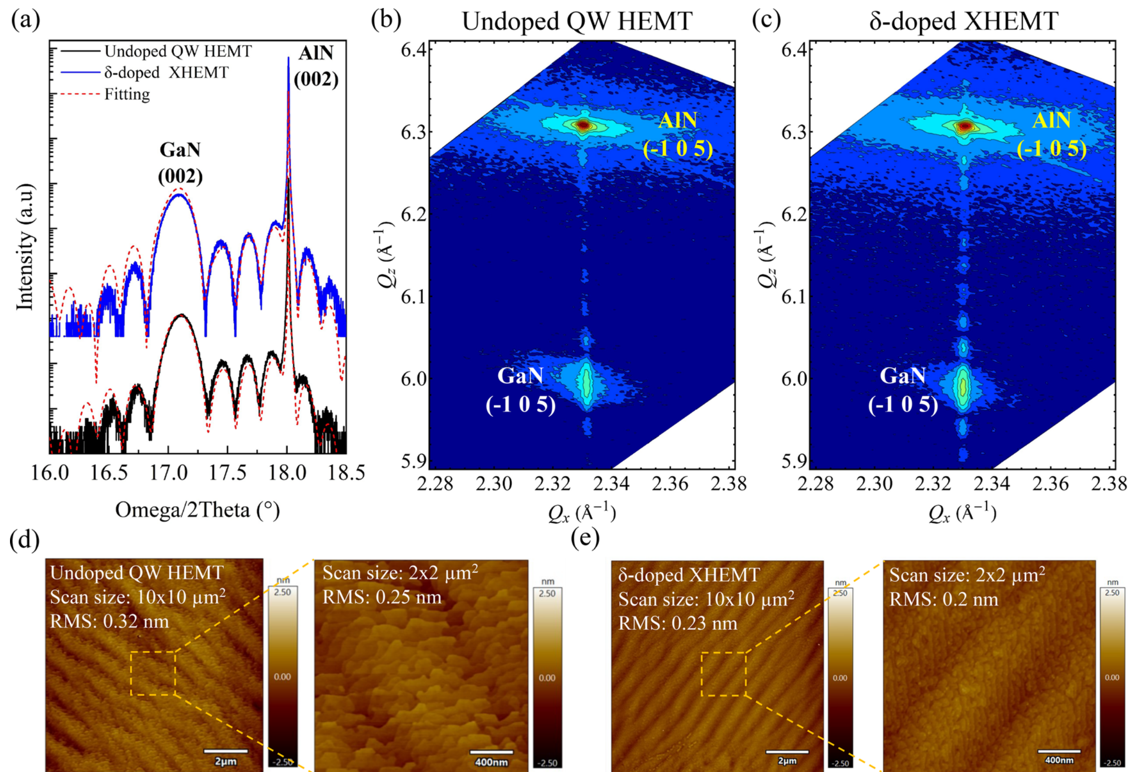

FIG. 2. (a) Measured (solid lines) and simulated (dashed lines) Omega/2Theta X-ray diffraction scans across the symmetric (002) reflection for both the undoped QW HEMT and δ-doped XHEMT, confirming the target thickness and sharp interfaces. (b) and (c) X-ray reciprocal space maps (RSMs) around the asymmetric (-105) reflection for the undoped QW HEMT and δ-doped XHEMT, respectively. Silicon δ-doping does not have a measurable structural impact on the strain state of the film. (d) and (e) $10 \times 10\,\mu m^2$ and $2 \times 2\,\mu m^2$ atomic force microscopy (AFM) scans of the as-grown undoped QW HEMT and δ-doped XHEMT, respectively, showing atomic steps and smooth surface morphologies.

TABLE I. The measured 2DEG densities (n_s), mobilities (μ) and sheet resistances (R_s) by Hall effect measurement at 290 and 10 K, and the calculated average electric field (F_{avg}) for the undoped QW HEMT and δ-doped XHEMT structures, respectively.

Sample	n_s^{290K} (10^{13} cm^{-2})	μ^{290K} (cm^2/Vs)	R_s^{290K} ($\Omega/\square$)	n_s^{10K} (10^{13} cm^{-2})	μ^{10K} (cm^2/Vs)	R_s^{10K} ($\Omega/\square$)	F_{avg} (MV/cm)
Undoped	2.04	611.1	501.9	2.01	1211.5	255.9	3.80
δ-doped	3.24	854.6	226.7	3.21	2240.2	86.86	2.84

from 611.1 cm^2/Vs in the undoped QW HEMT to 854.6 cm^2/Vs in the δ-doped XHEMT. At 10 K, the mobility rises from 1211.5 cm^2/Vs in the undoped QW HEMT to 2240.2 cm^2/Vs in the δ-doped XHEMT. As a result of the increased 2DEG density and mobility, the δ-doped XHEMT achieves a reduction in sheet resistance by over 2X, resulting in a RT sheet resistance of 226.7 $\Omega/\square$, as illustrated in Fig. 3(c).

One may expect that remote Coulomb scattering from donors at the δ-doped layer would degrade the mobility, which is clearly not observed experimentally. Through direct calculation, we find the effect of Coulomb scattering by the δ-dopants is negligible in this heterostructure compared to the phonon and IR scattering mechanisms that are shown in Fig. 3(b). Figure 3(b) also shows the calculated electron mobility with various scattering mechanisms against the experimentally measured temperature-dependent mobility, aiming to understand the physical origin underlying the improved electron mobility in the δ-doped XHEMT. For calculating mobilities, we used an electron effective mass $m_c^* = 0.25\, m_e$ measured by Shubnikov-de-Haas oscillations in these heterostructures, where m_e is the free electron mass. This slightly higher electron effective mass compared to standard AlGaN/GaN heterostructures with $m_c^* \approx 0.22\, m_e$[35–39] may be due to the nonparabolicity of electronic subband at high energies combined with the compressive strain in the GaN channel.[40] A comprehensive magnetotransport study of these heterostructures, including quantum oscillations that enable a measurement of m_c^*, will be presented in a future work. In the remaining part of this work, we discuss why δ-doping makes XHEMTs an attractive solution for high performance electronic devices.

03 October 2024 12:12:56

Published under an exclusive license by AIP Publishing

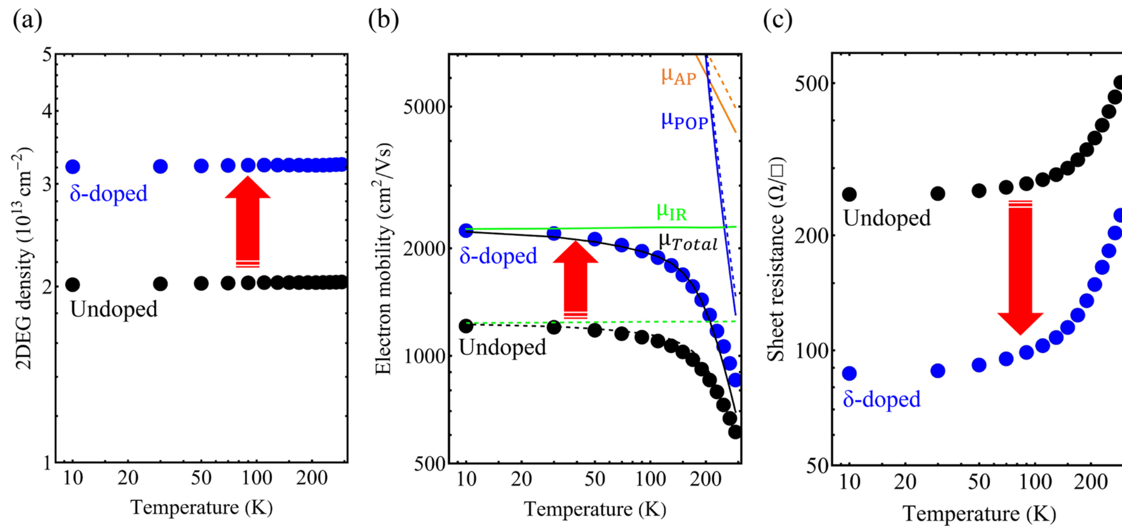

FIG. 3. Temperature-dependent (a) 2DEG density, (b) electron mobility and (c) sheet resistance for both the undoped QW HEMT (black circles) and δ-doped XHEMT (blue circles). The δ-doped XHEMT exhibits higher 2DEG density and electron mobility, resulting in a significant reduction in sheet resistance. Panel (b) includes a theoretical transport model. Dashed lines are scattering-limited mobilities for the undoped QW HEMT, while solid lines are those for the δ-doped XHEMT. The black lines are the total calculated mobility (μ_{Total}) according to Matthiessen's rule, combining contributions from three scattering mechanisms: acoustic phonon scattering (μ_{AP}, orange lines),[32] polar optical phonon scattering (μ_{POP}, blue lines),[33] and interface roughness scattering (μ_{IR}, green lines).[28,34]

In an earlier work, we identified IR scattering as the primary mobility-limiting factor in the undoped AlN/GaN/AlN heterostructures.[23] In Fig. 3(b), it is seen that the mobility lines limited by acoustic (AC)[32] and polar optical phonon (POP)[33] are similar for samples with and without δ-doping. The main difference at all temperatures is attributed to IR scattering[28,34] using the same correlation length $\Lambda = 1.25$ nm[41,42] for both samples, and the interface roughness parameter $\Delta = 0.27$ nm for the undoped QW HEMT, and $\Delta = 0.36$ nm for the δ-doped XHEMT. These (buried) interface roughness parameters are of the same order of magnitude as the experimentally measured rms surface roughness. The IR scattering rate depends quite strongly on the internal electric field (F_{avg}) and screening factor.[28] The average electric field at the electron wavefunction location is $F_{avg} = \frac{\int n(z)\times F(z)\,dz}{\int n(z)\,dz}$ where $n(z)$ and $F(z)$ are the local electron density and electric field respectively.[23,43] The introduction of δ-doping reduces F_{avg} by 25% from 3.80 MV/cm in the undoped QW HEMT to 2.84 MV/cm in the δ-doped XHEMT. The reduced F_{avg} moves the 2DEG centroid away from the interface. In addition, the increased 2DEG density in the δ-doped XHEMT enhances the screening of the scattering potential. These combined effects reduce IR scattering and enhance the channel mobility. Of particular note is the nearly doubled low-temperature electron mobility observed in the δ-doped XHEMT, attributed to reduced IR scattering. The elimination of the 2DHG removes potential drag effects and parallel conduction.

Figure 4 benchmarks the 2DEG density and RT mobility of the δ-doped XHEMT introduced in this work against previously reported coherently strained AlN/GaN/AlN heterostructures. The RT mobilities of undoped heterostructures were limited to 620 cm^2/Vs, as indicated by the black triangles[12,14,23] in Fig. 4. To address this limitation, initial enhancements were made by relaxing the GaN channel, resulting in RT electron mobility > 1000 cm^2/Vs and RT sheet resistance $< 300\,\Omega/\square$,[2,14,23] as shown by the gray circles in Fig. S1 in the supplementary material. But issues such as strain relief mediated by dislocation formation have been shown to cause increased dispersion and higher gate leakage currents in HEMTs.[44,45] Additionally, the high dislocation density in GaN enhances phonon-dislocation scattering, consequently decreasing its thermal conductivity.[46,47] In this work, δ-doped XHEMTs are seen to attain the highest RT mobility of 854.6 cm^2/Vs and lowest RT sheet resistance of 226.7 $\Omega/\square$ among all

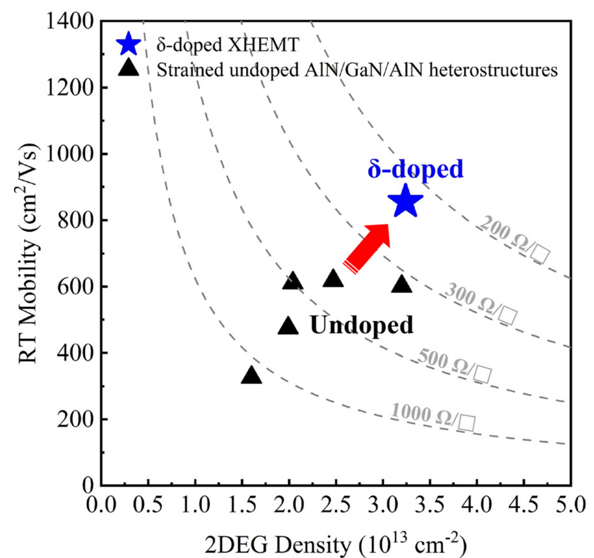

FIG. 4. Benchmark comparison of RT 2DEG density and mobility between the δ-doped XHEMT and previously reported coherently strained AlN/GaN/AlN heterostructures, with GaN QW thicknesses ranging from 14 to 20 nm.[12,14,23]

03 October 2024 12:12:56

Published under an exclusive license by AIP Publishing

coherently strained AlN/GaN/AlN heterostructures reported to date, without paying the penalty of relaxing the GaN channel and maintaining single-crystal properties throughout the whole heterostructure. To further enhance electron mobility in future heterostructure designs, advancements should build upon δ-doped XHEMT. Potential methods include reducing the 2DEG density and internal electric field in the well, which is achievable by replacing the AlN barrier with a coherently strained AlGaN barrier.

In summary, silicon δ-doping enhances the 2DEG density and mobility in AlN/GaN/AlN HEMT heterostructures without relaxing the GaN channel and forming dislocations. The δ-doped XHEMT, featuring a coherently strained GaN QW layer, is grown on a single-crystal AlN substrate. The δ-doping compensates 2DHGs and reduces the internal electric field in the well. This results in a high 2DEG density of 3.24×10^{13} cm^{-2} and a high RT mobility of 854.6 cm^2/Vs, leading to a RT sheet resistance of 226.7 $\Omega/\square$. The highest RT mobility and lowest sheet resistance in coherent, unrelaxed AlN/GaN/AlN HEMT heterostructures render them highly effective for RF and power electronics on the AlN platform. A large number of the channel transport advantages reported here by δ-doping in XHEMTs on single-crystal AlN substrates can also be enjoyed in AlN/GaN/AlN HEMTs with strained GaN QW channels on SiC, sapphire, or Si substrates.

See the supplementary material for the material parameters used for energy band diagram simulation and mobility calculations.

This work is supported by Army Research Office (Grant No. W911NF2220177) (Characterization); and ULTRA, an Energy Frontier Research Center funded by the U.S. Department of Energy (DOE), Office of Science, Basic Energy Sciences (BES), under Award No. DE-SC0021230 (Epitaxy). This work made use of the Cornell Center for Materials Research (CCMR) Shared Facilities which are supported through the NSF MRSEC program (DMR-1719875), CESI Shared Facilities partly sponsored by NSF No. MRI DMR-1631282, and Kavli Institute at Cornell (KIC).

AUTHOR DECLARATIONS

Conflict of Interest

The authors have no conflicts to disclose.

Author Contributions

Yu-Hsin Chen: Conceptualization (lead); Data curation (lead); Formal analysis (lead); Investigation (lead); Methodology (lead); Validation (lead); Writing – original draft (lead). **Jimy Encomendero:** Conceptualization (supporting); Investigation (supporting); Methodology (supporting); Validation (supporting). **Chandrashekhar Savant:** Investigation (supporting); Methodology (supporting). **Vladimir Protasenko:** Investigation (supporting); Methodology (supporting). **Huili (Grace) Xing:** Conceptualization (lead); Funding acquisition (lead); Investigation (supporting); Project administration (lead); Resources (lead); Supervision (lead); Writing – review & editing (supporting). **Debdeep Jena:** Conceptualization (lead); Funding acquisition (lead); Investigation (supporting); Project administration (lead); Resources (lead); Supervision (lead); Writing – review & editing (lead).

DATA AVAILABILITY

The data that support the findings of this study are available from the corresponding author upon reasonable request.

REFERENCES

[1] G. Li, R. Wang, J. Guo, J. Verma, Z. Hu, Y. Yue, F. Faria, Y. Cao, M. Kelly, T. Kosel *et al.*, "Ultrathin body GaN-on-insulator quantum well FETs with regrown Ohmic contacts," IEEE Electron Device Lett. **33**, 661–663 (2012).
[2] A. Hickman, R. Chaudhuri, L. Li, K. Nomoto, S. J. Bader, J. C. Hwang, H. G. Xing, and D. Jena, "First RF power operation of AlN/GaN/AlN HEMTs with >3 A/mm and 3 W/mm at 10 GHz," IEEE J. Electron Devices Soc. **9**, 121–124 (2021).
[3] R. Rounds, B. Sarkar, A. Klump, C. Hartmann, T. Nagashima, R. Kirste, A. Franke, M. Bickermann, Y. Kumagai, Z. Sitar *et al.*, "Thermal conductivity of single-crystalline AlN," Appl. Phys. Express **11**, 071001 (2018).
[4] A. Hickman, R. Chaudhuri, S. J. Bader, K. Nomoto, K. Lee, H. G. Xing, and D. Jena, "High breakdown voltage in RF AlN/GaN/AlN quantum well HEMTs," IEEE Electron Device Lett. **40**, 1293–1296 (2019).
[5] E. Kim, Y.-H. Chen, J. Encomendero, D. Jena, and H. G. Xing, "AlN/GaN/AlN HEMTs on bulk AlN substrates with high drain current density$>$ 2.8 A/mm and average breakdown field$>$ 2 MV/cm," in *Device Research Conference (DRC)* (IEEE, 2024), pp. 1–2.
[6] M. A. Khan, J. Kuznia, J. Van Hove, N. Pan, and J. Carter, "Observation of a two-dimensional electron gas in low pressure metalorganic chemical vapor deposited GaN-$Al_xGa_{1-x}N$ heterojunctions," Appl. Phys. Lett. **60**, 3027–3029 (1992).
[7] X. Hu, J. Deng, N. Pala, R. Gaska, M. Shur, C. Chen, J. Yang, G. Simin, M. A. Khan, J. Rojo *et al.*, "AlGaN/GaN heterostructure field-effect transistors on single-crystal bulk AlN," Appl. Phys. Lett. **82**, 1299–1301 (2003).
[8] E. Kim, Z. Zhang, J. Encomendero, J. Singhal, K. Nomoto, A. Hickman, C. Wang, P. Fay, M. Toita, D. Jena *et al.*, "N-polar GaN/AlGaN/AlN high electron mobility transistors on single-crystal bulk AlN substrates," Appl. Phys. Lett. **122**, 092104 (2023).
[9] G. Alvarez-Escalante, R. Page, R. Hu, H. G. Xing, D. Jena, and Z. Tian, "High thermal conductivity and ultrahigh thermal boundary conductance of homoepitaxial AlN thin films," APL Mater. **10**, 011115 (2022).
[10] S. Rennesson, M. Leroux, M. Al Khalfioui, M. Nemoz, S. Chenot, J. Massies, L. Largeau, E. Dogmus, M. Zegaoui, F. Medjdoub *et al.*, "Ultrathin AlN-based HEMTs grown on silicon substrate by NH_3-MBE," Phys. Status Solidi A **215**, 1700640 (2018).
[11] S. Patwal, M. Agrawal, K. Radhakrishnan, T. L. A. Seah, and N. Dharmarasu, "Enhancement of 2D electron gas mobility in an AlN/GaN/AlN double-heterojunction high-electron-mobility transistor by epilayer stress engineering," Phys. Status Solidi A **217**, 1900818 (2020).
[12] M. Qi, G. Li, S. Ganguly, P. Zhao, X. Yan, J. Verma, B. Song, M. Zhu, K. Nomoto, H. G. Xing *et al.*, "Strained GaN quantum-well FETs on single crystal bulk AlN substrates," Appl. Phys. Lett. **110**, 063501 (2017).
[13] S. Islam, M. Qi, B. Song, K. Nomoto, V. Protasenko, J. Wang, S. Rouvimov, P. Fay, H. G. Xing, and D. Jena, "First demonstration of strained AlN/GaN/AlN quantum well FETs on SiC," in *74th Annual Device Research Conference* (IEEE, 2016), pp. 1–2.
[14] R. Chaudhuri, *Integrated Electronics on Aluminum Nitride: Materials and Devices* (Springer Nature, 2022).
[15] J. Yaita, K. Fukuda, A. Yamada, T. Iwasaki, S. Nakaharai, and J. Kotani, "Improved channel electron mobility through electric field reduction in GaN quantum-well double-heterostructures," IEEE Electron Device Lett. **42**, 1592–1595 (2021).
[16] Z. Fan, J. Li, M. Nakarmi, J. Lin, and H. Jiang, "AlGaN/GaN/AlN quantum-well field-effect transistors with highly resistive AlN epilayers," Appl. Phys. Lett. **88**, 073513 (2006).
[17] R. Chaudhuri, S. J. Bader, Z. Chen, D. A. Muller, H. G. Xing, and D. Jena, "A polarization-induced 2D hole gas in undoped gallium nitride quantum wells," Science **365**, 1454–1457 (2019).
[18] Z. Zhang, J. Encomendero, R. Chaudhuri, Y. Cho, V. Protasenko, K. Nomoto, K. Lee, M. Toita, H. G. Xing, and D. Jena, "Polarization-induced 2D hole gases

03 October 2024 12:12:56

Published under an exclusive license by AIP Publishing

in pseudomorphic undoped GaN/AlN heterostructures on single-crystal AlN substrates," Appl. Phys. Lett. **119**, 162104 (2021).
[19]G. Li, B. Song, S. Ganguly, M. Zhu, R. Wang, X. Yan, J. Verma, V. Protasenko, H. Grace Xing, and D. Jena, "Two-dimensional electron gases in strained quantum wells for AlN/GaN/AlN double heterostructure field-effect transistors on AlN," Appl. Phys. Lett. **104**, 193506 (2014).
[20]H. Condori Quispe, S. Islam, S. Bader, A. Chanana, K. Lee, R. Chaudhuri, A. Nahata, H. Xing, D. Jena, and B. Sensale-Rodriguez, "Terahertz spectroscopy of an electron-hole bilayer system in AlN/GaN/AlN quantum wells," Appl. Phys. Lett. **111**, 073102 (2017).
[21]M. Kane, N. Apsley, D. Anderson, L. Taylor, and T. Kerr, "Parallel conduction in GaAs/Al_xGa_{1-x}As modulation doped heterojunctions," J. Phys. C **18**, 5629 (1985).
[22]R. Höpfel, J. Shah, P. Wolff, and A. Gossard, "Electron-hole scattering in GaAs quantum wells," Phys. Rev. B **37**, 6941 (1988).
[23]Y.-H. Chen, J. Encomendero, C. Savant, V. Protasenko, H. G. Xing, and D. Jena, "Electron mobility enhancement by electric field engineering of AlN/GaN/AlN quantum-well HEMTs on single-crystal AlN substrates," Appl. Phys. Lett. **124**, 152111 (2024).
[24]S. Rajan, A. Chini, M. H. Wong, J. S. Speck, and U. K. Mishra, "N-polar GaN/AlGaN/GaN high electron mobility transistors," J. Appl. Phys. **102**, 044501 (2007).
[25]M. H. Wong, U. Singisetti, J. Lu, J. S. Speck, and U. K. Mishra, "Anomalous output conductance in N-polar GaN high electron mobility transistors," IEEE Trans. Electron Devices **59**, 2988–2995 (2012).
[26]C. A. Schaake, *Contributions to the Science and Technology of Enhancing the Internal Quantum Efficiency of Nitride Light Emitting Diodes* (University of California, Santa Barbara, CA, 2009).
[27]H. Li, S. Wienecke, B. Romanczyk, E. Ahmadi, M. Guidry, X. Zheng, S. Keller, and U. K. Mishra, "Enhanced mobility in vertically scaled N-polar high-electron-mobility transistors using GaN/InGaN composite channels," Appl. Phys. Lett. **112**, 073501 (2018).
[28]U. Singisetti, M. Hoi Wong, and U. K. Mishra, "Interface roughness scattering in ultra-thin N-polar GaN quantum well channels," Appl. Phys. Lett. **101**, 012101 (2012).
[29]R. T. Bondokov, S. P. Branagan, N. Ishigami, J. Grandusky, T. Nagatomi, K. Tatsuta, T. Miebach, and J. J. Chen, "Two-inch aluminum nitride (AIN) single crystal growth for commercial applications," ECS Trans. **104**, 37 (2021).
[30]K. Lee, Y. Cho, L. J. Schowalter, M. Toita, H. G. Xing, and D. Jena, "Surface control and MBE growth diagram for homoepitaxy on single-crystal AlN substrates," Appl. Phys. Lett. **116**, 262102 (2020).
[31]Y. Cho, C. S. Chang, K. Lee, M. Gong, K. Nomoto, M. Toita, L. J. Schowalter, D. A. Muller, D. Jena, and H. G. Xing, "Molecular beam homoepitaxy on bulk AlN enabled by aluminum-assisted surface cleaning," Appl. Phys. Lett. **116**, 172106 (2020).
[32]J. H. Davies, *The Physics of Low-Dimensional Semiconductors: An Introduction* (Cambridge University Press, 1998).
[33]B. Gelmont, M. Shur, and M. Stroscio, "Polar optical-phonon scattering in three-and two-dimensional electron gases," J. Appl. Phys. **77**, 657–660 (1995).
[34]R. K. Jana and D. Jena, "Stark-effect scattering in rough quantum wells," Appl. Phys. Lett. **99**, 012104 (2011).
[35]L. Wong, S. Cai, R. Li, K. Wang, H. Jiang, and M. Chen, "Magnetotransport study on the two-dimensional electron gas in AlGaN/GaN heterostructures," Appl. Phys. Lett. **73**, 1391–1393 (1998).
[36]S. Elhamri, R. Newrock, D. Mast, M. Ahoujja, W. Mitchel, J. Redwing, M. Tischler, and J. Flynn, "$Al_{0.15}Ga_{0.85}N$/GaN heterostructures: Effective mass and scattering times," Phys. Rev. B **57**, 1374 (1998).
[37]A. Saxler, P. Debray, R. Perrin, S. Elhamri, W. Mitchel, C. Elsass, I. Smorchkova, B. Heying, E. Haus, P. Fini *et al.*, "Characterization of an AlGaN/GaN two-dimensional electron gas structure," J. Appl. Phys. **87**, 369–374 (2000).
[38]A. Brana, C. Diaz-Paniagua, F. Batallan, J. Garrido, E. Munoz, and F. Omnes, "Scattering times in AlGaN/GaN two-dimensional electron gas from magnetoresistance measurements," J. Appl. Phys. **88**, 932–937 (2000).
[39]T. Wang, J. Bai, S. Sakai, Y. Ohno, and H. Ohno, "Magnetotransport studies of AlGaN/GaN heterostructures grown on sapphire substrates: Effective mass and scattering time," Appl. Phys. Lett. **76**, 2737–2739 (2000).
[40]A. Kurakin, S. Vitusevich, S. Danylyuk, H. Hardtdegen, N. Klein, Z. Bougrioua, A. Naumov, and A. Belyaev, "Quantum confinement effect on the effective mass in two-dimensional electron gas of AlGaN/GaN heterostructures," J. Appl. Phys. **105**, 073703 (2009).
[41]Y. Cao and D. Jena, "High-mobility window for two-dimensional electron gases at ultrathin AlN/GaN heterojunctions," Appl. Phys. Lett. **90**, 182112 (2007).
[42]Y. Zhang, I. Smorchkova, C. Elsass, S. Keller, J. P. Ibbetson, S. Denbaars, U. K. Mishra, and J. Singh, "Charge control and mobility in AlGaN/GaN transistors: Experimental and theoretical studies," J. Appl. Phys. **87**, 7981–7987 (2000).
[43]Z. Zhang, J. Encomendero, E. Kim, J. Singhal, Y. Cho, K. Nomoto, M. Toita, H. G. Xing, and D. Jena, "High-density polarization-induced 2D electron gases in N-polar pseudomorphic undoped GaN/$Al_{0.85}Ga_{0.15}N$ heterostructures on single-crystal AlN substrates," Appl. Phys. Lett. **121**, 082107 (2022).
[44]M. Ťapajna, S. Kaun, M. Wong, F. Gao, T. Palacios, U. Mishra, J. Speck, and M. Kuball, "Influence of threading dislocation density on early degradation in AlGaN/GaN high electron mobility transistors," Appl. Phys. Lett. **99**, 223501 (2011).
[45]S. W. Kaun, M. H. Wong, S. Dasgupta, S. Choi, R. Chung, U. K. Mishra, and J. S. Speck, "Effects of threading dislocation density on the gate leakage of AlGaN/GaN heterostructures for high electron mobility transistors," Appl. Phys. Express **4**, 024101 (2011).
[46]H. Li, R. Hanus, C. A. Polanco, A. Zeidler, G. Koblmüller, Y. K. Koh, and L. Lindsay, "GaN thermal transport limited by the interplay of dislocations and size effects," Phys. Rev. B **102**, 014313 (2020).
[47]K. Termentzidis, M. Isaiev, A. Salnikova, I. Belabbas, D. Lacroix, and J. Kioseoglou, "Impact of screw and edge dislocations on the thermal conductivity of individual nanowires and bulk GaN: A molecular dynamics study," Phys. Chem. Chem. Phys. **20**, 5159–5172 (2018).

03 October 2024 12:12:56

Published under an exclusive license by AIP Publishing